Engineering Journal issn: 0125-8281

Article

Trajectory Tracking Control Design for Dual-Arm Robots Using Dynamic Surface Controller

Anh Tuan Phan[1,a,*], Huu Nguyen Thai[2], Cong Khoa Nguyen[1], Quang Uoc Ngo[3], Hoai Anh Duong[1], and Quoc Truong Vo[1]

1 Hanoi University of Science and Technology, Hanoi, 10000, Vietnam
2 Vinh University of Technology Education, Vinh, 43100, Vietnam
3 Vietnam National University of Agriculture, Hanoi, 10000, Vietnam
E-mail: [a]anhtuanphan2510@gmail.com (Corresponding author)

Abstract. This paper presents a dynamic surface controller (DSC) for dual-arm robots (DAR) tracking desired trajectories. The DSC algorithm is based on backstepping technique and multiple sliding surface control principle, but with an important addition. In the design of DSC, low-pass filters are included which prevent the complexity in computing due to the "explosion of terms", i.e. the number of terms in the control law rapidly gets out of hand. Therefore, a controller constructed from this algorithm is simulated on a four degrees of freedom (DOF) dual-arm robot with a complex kinetic dynamic model. Moreover, the stability of the control system is proved by using Lyapunov theory. The simulation results show the effectiveness of the controller which provide precise tracking performance of the manipulator.

Keywords: Backstepping, multi sliding surface control, dynamic surface control, dual arm robot, manipulators.

ENGINEERING JOURNAL Volume 24 Issue 3
Received 4 December 2019
Accepted 15 April 2020
Published 31 May 2020
Online at https://engj.org/
DOI:10.4186/ej.2020.24.3.159

This article is based on the presentation at The 2019 First International Symposium on Instrumentation, Control, Artificial Intelligence, and Robotics (ICA-SYMP 2019) in Bangkok, Thailand, 16 - 18 January 2019.

DOI:10.4186/ej.2020.24.3.159

1. Introduction

Robotic systems are increasingly used in a vast range of heavy industrial plants, even in the habitual human life [1, 2, 3, 4, 5, 6]. In fact, in many manufactories, manipulators have taken the place of human workers to transfer and assemble machineries and devices on production lines because they own the ability of handling large objects. Robotic systems, they will be especially preferred if the working conditions are extremely harsh and dangerous such as space tasks or nuclear power plants. In medical care and household chores, humanoid robots capable of speaking and interacting with people are gradually applied. Therefore, the issues of cooperative motion control of manipulators have significantly attracted the researchers in recent years.

In spite of the flexibility and versatility in task execution, it is much more difficult to control of the dual-arm cooperative manipulators than that of single arm robot. While singe-arm manipulator (SAM) shows open kinematic modeling, dual-arm manipulator (DAM) remains complex dynamic coupling and kinematic redundancy. A difficult part, but integral of DAM is how to automate motion planning concerned with the determination of optimal position and force trajectories of individual arms under the kinesthetic constraints imposed by dual-arm cooperation. The complexity in the manipulation of DAM also comes from the necessity to control the kinematic and dynamic interactions between the two arms to accomplish the planned position and force trajectories. These problems have significant attention from the researchers who are interested in robotic systems. Many control strategies with the aim of ensuring a good tracking performance on the robot trajectory have been published. Wen et al. [7] proposed a motion and force control technique for operating a multiple arm robot system. While Perdereau and Drouin analyzed a hybrid external control of two cooperative manipulators in paper [8]. Besides the impedance control method was applied to the dual-arm robots in papers [9, 10]. Such the control methods [7, 8, 9, 10] are not effective in case of unexpected emergence of disturbances and obstacles in the robot system's workspace. Because of that, it is required a robust and reliable controller so as to maintain the desired motion trajectory.

Some researchers utilized variable structure control (VSC) as known as sliding mode control (SMC) approach [11] to deal with the robotic system's insensitivity to external disturbances and parameter variations. In this control method, the states of the system are directed to reach a predetermined switching surface after which they are forced to "slide"' along or nearby the vicinity of the surface by means of a sliding motion. While sliding, the system is insensitive to parameter variations and external disturbances. In paper [12] Yagiz et al. proposed sliding mode controller (SMC) applied on a dual-arm robot. After that, they developed the controller by combining with fuzzy logic technique which took responsible for regulating the gains of SMC law in paper [13]. While Joo et al. constructed an adaptive control system based on adaptive neural network control with SMC for DAM in paper [14]. However, one of the inevitable disadvantages of SMC is undesirable chattering phenomenon. It may break actuators or sometimes make the system unstable.

Besides, the backstepping control is considered as a popular technique in nonlinear system design since the derived system control law and parameters adaptive law are able to make controlled system be global stable and robust. Using adaptive backstepping technique, the authors in paper [15] designed a controller for robot manipulator with the aim of trajectory tracking. Paper [16] Nikdel et al. integrated an adaptive backstepping control approach into fractional-order controller design for robotic system. While the stability of the controlled system can be guaranteed by Lyapunov stability theorem. Moreover, some authors utilized backstepping technique combining with modern control methods such as fuzzy logic [17, 18], neural netwwork [19, 20, 21] applied for manipulators treat well the problems of uncertainties and unmodeled systems. In spite of this, there is increase in complexity of the regression matrices and over-parametrization with each step of the backstepping process.

Based on sliding mode control and backstepping techniques, D. Swaroop et al. proposed DSC algorithm [22] which ensured exponential regulation and bounded tracking error. This method not only inherited the robustness of the aforementioned techniques but also reduced the explosion of terms. Because there were low-pass filters in controller design, the model was not differentiated, at the same time, avoiding complexity arising in the operation. Some researchers applied DSC to control of nonlinear systems [23, 24]. The controller quality is verified in some circumstances with unexpected disturbances affecting to the controlled signal.

In this paper, we proposed dynamic surface controller for dual arm robot system in handling and transporting a payload follow a desired trajectory. The controller quality is verified in some circumstances with unexpected disturbances affecting to the controlled signal. Moreover, the presence of the

auxiliary first-order filters in design removes the need for differentiation and reduces the explosion of terms which make the simulation faster and better. In addition, the stability of the closed-loop system is guaranteed by Lyapunov theory. The rest of the paper includes 5 sections. In Section 2, the physical model of the dual arm robotic system is constructed. In Section 3, DSC for robot is introduced. Section 4 shows simulation results. Section 5 and section 6 are conclusion and appendix.

2. System Modelling

In this paper, the model of DAM will be constructed as the robot arm's physical model in paper [12]. Fig.1 illustrates a model of cooperative robotic system consists of two planar robot arms within 4 DOF. The manipulators are handling an object and its weight is m. In the physical model, m_i, I_i and L_i represents respectively the mass, mass moment of inertia and length of the related links $\left(i=\overline{1,4}\right)$. While the width of the rectangular load is d_1 and the distance between the base of the robot arms is d_2. The distance of the mass center of the related link to the preceding joint and the joint angle of the related link are represented as k_i and θ_i respectively. In addition, b_i is used to denote the viscous frictions acting on all of the joints. In order to define the trajectory of both arms, we have:

$$\begin{aligned} x_m &= d_2/2 \ + L_1\cos\theta_1 + L_2\cos(\theta_1+\theta_2) - d_1/2 \\ &= -d_2/2 \ + L_3\cos\theta_3 + L_4\cos\left(\theta_3+\theta_4\right) + d_1/2 \end{aligned} \tag{1}$$

$$\begin{aligned} y_m &= L_1\sin\theta_1 + L_2\sin\left(\theta_1+\theta_2\right) \\ &= L_3\sin\theta_3 + L_4\sin\left(\theta_3+\theta_4\right) \end{aligned} \tag{2}$$

While performing the transportation task, the robot applies forces F_1, F_2 from its end effectors to the load as shown in Fig.2. The friction forces F_{s1}, F_{s2} and their components F_{s1y}, F_{s1z}, F_{s2y}, F_{s2z} between the arm tips and the load surface prevent the load sliding during motion. Here μ represents the coefficient of dry friction. In this study it is deemed that the load be moved without rotation so that F_{s1y} and F_{s2y} are equal, preventing rotation about z-axis. In addition, F_{s1z} and F_{s2z} also are equal, since there is to be no rotation about y-axis, either.

The dynamic equations of the load are:

$$\begin{aligned} m\ddot{x}_m &= F_2 - F_1 \\ m\ddot{y}_m &= 2F_{s1y} = 2F_{s2y} \\ mg &= 2F_{s1z} = 2F_{s2z} \end{aligned} \tag{3}$$

and the expressions for friction forces are:

$$F_{s1y}{}^2 + \left(\frac{m.g}{2}\right)^2 < (\mu F_1)^2 \tag{4}$$

$$F_{s2y}{}^2 + \left(\frac{m.g}{2}\right)^2 < (\mu F_2)^2 \tag{5}$$

Since the direction of the forces F_1, F_2 are always set towards the load so that the load can be effectively handled, these forces should be positive. Therefore, the friction force equation, which yields a positive signed solution for both F_1 and F_2 should be chosen. In this research the following solutions were used. If the acceleration of the load in the x-direction is equal to or greater than zero $\left(\ddot{x}_{m(t)} \geq 0\right)$ then using Eq.(4) , the following relations for F_1 and F_2 are obtained.

$$\begin{aligned} F_1 &= \frac{1}{\mu}\sqrt{\left(\frac{m.\ddot{y}_m}{2}\right)^2 + \left(\frac{m.g}{2}\right)^2} \\ F_2 &= \frac{1}{\mu}\sqrt{\left(\frac{m.\ddot{y}_m}{2}\right)^2 + \left(\frac{m.g}{2}\right)^2} + m.\ddot{x}_m \end{aligned} \tag{6}$$

Here, since $\ddot{x}_{m(t)} \geq 0$ is satisfied, the interaction forces F_1 and F_2 are both positive. If $\ddot{x}_{m(t)} \leq 0$, Eq.(5) is used and the following relations for the interaction forces are obtained.

$$\begin{aligned} F_1 &= \frac{1}{\mu}\sqrt{\left(\frac{m.\ddot{y}_m}{2}\right)^2 + \left(\frac{m.g}{2}\right)^2} - m.\ddot{x}_m \\ F_2 &= \frac{1}{\mu}\sqrt{\left(\frac{m\ddot{y}_m}{2}\right)^2 + \left(\frac{mg}{2}\right)^2} \end{aligned} \tag{7}$$

Here, since $\ddot{x}_{m(t)} \leq 0$ is satisfied, the interaction forces F_1 and F_2 are both positive.

By using Euler Lagrange modeling for system, we obtain the system dynamic of dual arm robot when operating with the payload can be simplified in vector form as:

$$\begin{aligned} &M(\theta)\ddot{\theta} + C(\theta,\dot{\theta})\dot{\theta} + G(\theta) \\ &= u + J^T(\theta)F(\theta,\dot{\theta},\ddot{\theta}) - W - d \end{aligned} \tag{8}$$

Here, $M(\theta)$ is a 4x4 inertial matrix, $C(\theta,\dot{\theta})$ is a 4x1 Coriolis-centripetal vector, u is a 4x1 control torque input vector, $F(\theta,\dot{\theta},\ddot{\theta})$ is a 4x1 vector indicating interaction forces between object and robot arms, J is a 4x 4 Jacobian matrix, W is a 4x1 vector including the noise effects on robot arms and d denotes viscous friction forces on all joint. The details of Eq.(8) are given in the Appendix.

DOI:10.4186/ej.2020.24.3.159

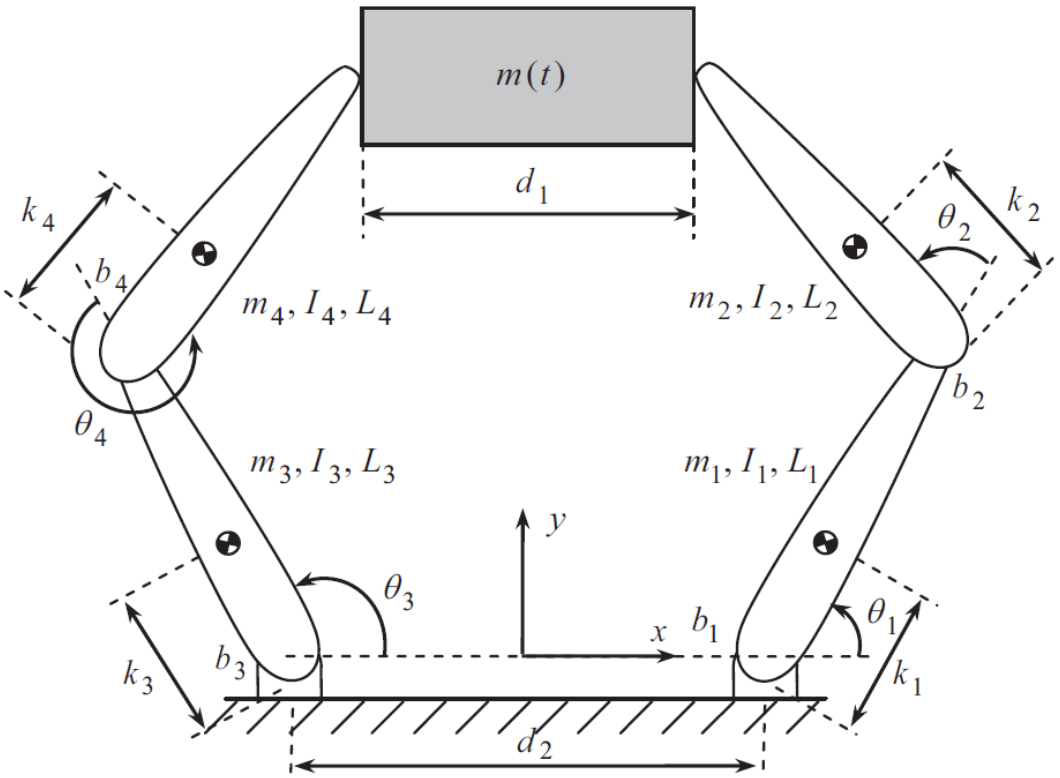

Fig. 1. The 4 DOF dual arm robot model.

3. Designing Controller For Dual-Arm Robot

3.1. Dynamic Surface Control

The DSC algorithm are based on backstepping and multiple sliding surface control (MSSC) methods, but with an important addition that is an included low pass filter in the design. The following example illustrates the DSC approach for a nonlinear system:

$$\begin{cases} \dot{x}_1 = x_2 + f(x_1) \\ \dot{x}_2 = u \end{cases} \tag{9}$$

where the function $f(x_1)$ is non-Lipschitz nonlinearity and is assumed completely known. We define the sliding surfaces as follows:

$$S_1 = x_1 - x_{1d} \tag{10}$$

$$S_2 = x_2 - x_{2d} \tag{11}$$

$$\Rightarrow \dot{S}_1 = S_2 + x_{2d} + f(x_1) - \dot{x}_{1ref} \tag{12}$$

Then we choose x_{2d} to make $S_1.\dot{S}_1 < 0$ assuming S_2 will be driven to zero.

We define a virtual control signal $\bar{x}_2$ as follows:

$$\bar{x}_2 = x_{1d} - f(x_1) - c_1.S_1 \tag{13}$$

If x_2 were to track $\bar{x}_2$ asymptotically, S_1 would converge to a neighborhood about 0. In order to avoid the problem faced by the multiple surface sliding scheme, $\bar{x}_2$ is passed through a first order filter:

$$\begin{cases} \tau.\dot{x}_{2d} + x_{2d} = \bar{x}_2 \\ x_{2d}(0) = \bar{x}_2(0) \end{cases} \tag{14}$$

Now, u is chosen to drive S_2 to zero

$$u = \dot{\alpha}_{2f} - c_2 S_2 = \frac{\alpha - \alpha_{2f}}{\tau} - c_2 S_2 \tag{15}$$

where c_1 and c_2 are positive matrix.

The Lyapunov function is defined as follows:

$$V = \frac{S_1^2 + S_2^2}{2} \tag{16}$$

The proving for the stability will be discuss in the specific followed system. The significant difference of DSC in comparison with MSSC or Backstepping is the low-pass filter (14) which reduces the explosion of terms.

3.2. Dynamic Surface Controller For Dual–Arm Robot

A robust control system will be designed for 4 DOFs dual-arm robot of which the model is written as:

$$\begin{cases} \dot{x}_1 = x_2 \\ \dot{x}_2 = M^{-1}(\theta).u + M^{-1}(\theta).K(\theta, \dot{\theta}, \ddot{\theta}) \end{cases} \tag{17}$$

DOI:10.4186/ej.2020.24.3.159

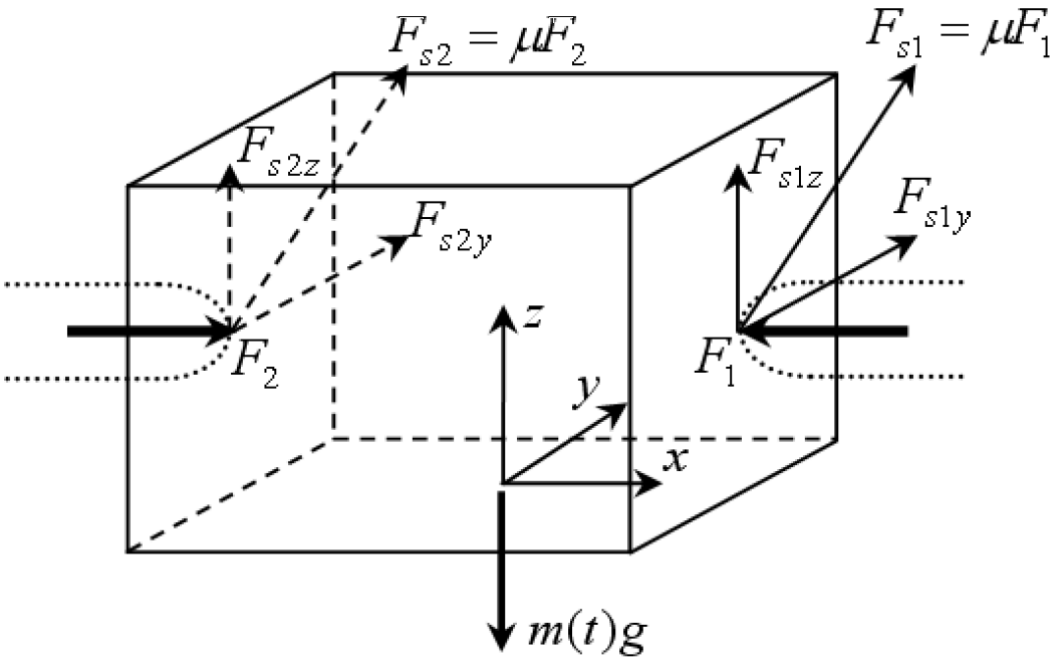

Fig. 2. The impact force on the load.

where $x_1 = (\theta_1, \theta_2, \theta_3, \theta_4)^T$ and $K(\theta, \dot{\theta}, \ddot{\theta}) = -J^T(\theta).F(\theta, \dot{\theta}, \ddot{\theta}) - C(\theta, \dot{\theta}) - G(\theta) - \beta - W$.

The first sliding surface is defined as follows:

$$S_1 = x_1 - x_{1d} \tag{18}$$

$$\Rightarrow \dot{S}_1 = \dot{x}_1 - \dot{x}_{1d} = x_2 - \dot{x}_{1d} \tag{19}$$

where $x_{1d} = \theta_{ref}$ is the reference value of joint angles.

Define the second surface as follows:

$$S_2 = x_2 - x_{2d} \tag{20}$$

with x_{2d} is the virtual control tracking to $\bar{x}_2$ through a filter $\tau.\dot{x}_{2d} + x_{2d} = \bar{x}_2$ while $x_{2d}(0) = \bar{x}_2(0)$ and constant time $\tau > 0$.

The second Lyapunov Candidate Function is defined as:

$$V = \frac{1}{2}S_1^T S_1 + \frac{1}{2}S_2^T S_2 \tag{21}$$

$$\begin{aligned}\dot{V} &= -S_1^T c_1 S_1 + S_1^T S_2 + S_2^T \dot{S}_2 \\ &= -S_1^T c_1 S_1 + S_2^T (S_1 + M^{-1}u \\ &\quad + M^{-1}K - \dot{x}_{2d})\end{aligned} \tag{22}$$

The final control signal is chosen as:

$$\underline{u} = -K - M(S_1 + c_2 S_2 - \dot{x}_{2d}) \tag{23}$$

where c_1 , c_2 are positive matrix.

So that, we have $\dot{V}_2 = -S_1^T c_1 S_1 - S_2^T c_2 S_2$ is negative defined, equivalently the system errors asymptotically converge to zero as $t \to \infty$.

4. Simulation Results And Discussion

For numerical demonstration of the proposed method's performance through the dynamic system of the DAM, the simulation model of the controller and the DAM are built and verified in MATLAB application. There are two stages in the motion of the robot arms, namely approaching and transportation. Initially the robot arms are at rest with initial values of the joint angles given in Table 1, then they approach to the load gradually. After picking up, they transport the load to new location appointed. The reference trajectories of the robot arm tips for approaching motion are defined in Eq.(24).

$$\begin{cases} x_{p1r}(t) = x_{f1} + (x_{i1} - x_{f1})e^{-10t^2} \\ y_{p1r}(t) = y_{f1} + (y_{i1} - y_{f1})e^{-10t^2} \\ x_{p2r}(t) = x_{f2} + (x_{i2} - x_{f2})e^{-10t^2} \\ y_{p2r}(t) = y_{f2} + (y_{i2} - y_{f2})e^{-10t^2} \end{cases} \tag{24}$$

Here p_1 and p_2 denote the endpoints of the first and second robot arms, respectively. Also, in the approaching motion, (x_i, y_i) and (x_f, y_f) are initial and final coordinates of robot end-effectors for approaching motion.

Additionally, the reference trajectories for the coordinates of the load center during the transportation motion are defined in Eq.(25) and Eq.(26):

$$x_{mr}(t) = \begin{cases} x_p & ; t < 2 \\ x_f + (x_i - x_f)e^{-10.(t-2)^2} & ; t \geq 2 \end{cases} \tag{25}$$

DOI:10.4186/ej.2020.24.3.159

Table 1. Parameters of the dual arm robot system.

Parameters of DAR dynamic model
$m_1 = m_2 = m_3 = m_4 = 1.5\,(kg)$; $m = 1\,(kg)$;
$I_1 = I_2 = I_3 = I_4 = 0.18\,(kgm^2)$;
$L_1 = L_2 = L_3 = L_4 = 1.2\,(m)$;
$k_1 = k_2 = k_3 = k_4 = 0.48\,(m)$;
$b_1 = b_2 = b_3 = b_4 = 110\,(Nm/s)$;
$d_1 = 0.25\,(m)$; $d_2 = 1.2\,(m)$; $\mu = 0.35$
Generated path – Initial condition
$(x_{i1},\, y_{i1}) = (0.76,\, 0.6)$; $(x_{i2},\, y_{i2}) = (-0.76,\, 0.6)$;
$(x_{f1},\, y_{f1}) = (-0.275,\, 1.4)$; $(x_{f2},\, y_{f2}) = (-0.525,\, 1.4)$;
$(x_0, y_0) = (0,\, 1.4)$; $r_m = 0.4$;
$\theta_1(0) = 0$; $\theta_2(0) = \frac{\pi}{2}$; $\theta_3(0) = \pi$; $\theta_4(0) = \frac{-\pi}{2}$;
$\dot{\theta}_1(0) = \dot{\theta}_2(0) = \dot{\theta}_3(0) = \dot{\theta}_4(0) = 0$
Parameters of dynamic surface controller
$\lambda = diag\,(10, 10, 10, 10)$; $\sigma = 10^{-10}$
$c_1 = diag\,(50, 50, 50, 50)$; $c_2 = diag\,(50, 50, 50, 50)$

$$y_{mr}(t) = \begin{cases} y_p & ;t < 2 \\ y_f + (y_i - y_f)e^{-10.(t-2)^2} & ;t \geq 2 \end{cases} \quad (26)$$

In the simulation experiments, the dynamic models of the dual arm robot were given. Moreover, the parameters of dual-arm robot and the proposed controllers are summarized in Table 1.

In the simulation, we verify the controller performance with external disturbance affecting control signals of the robot's joints as shown in Fig.3. In addition, we compare the performance of the controller to that of Sliding Mode Controller (SMC).

To examine the effectiveness of the proposed technique, we will investigate motions of the four links and the motion trajectories of the two end effectors of DAR.

At first, Fig. 4 describes the actual angles of all robot's joints along with their reference which is delineated on $xy - plane$. It can be clearly seen that for the purposes of comparisons, in this experimental example we implemented two algorithms including the classical SMC [12] and the proposed method DSC introduced in Section 3. The results obtained by the two implemented approaches are expected to reach the references. Both the SMC and DSC make the robot's arms track their desired trajectories even with external disturbances.

Next, for the motion trajectories of the two end effectors as demonstrated in Fig. 5, it shows that the proposed approach is effectively practical. All arm tip's trajectory approach and track the desired trajectory with high accuracy.

5. Conclusion

We have proposed a controller for dual arm robot based one dynamic surface control. The simulation results show that the presented control method is able to ensure the stability and tracking performance for the DAM system. The DSC responses show better quality in comparision with SMC responses. Futhermore, the controller provide a high robustness and acuratecy in the condition that the unknown disturbance is existed. Therefore, the DSC can be recommended for nonlinear systems requiring high accuracy and safe transportation.

6. Appendix

The vectors used in the equation (8) of motion of 4-DOF dual-arm robot:

$$u = \begin{bmatrix} u_1 & u_2 & u_3 & u_4 \end{bmatrix}^T;$$
$$F = \begin{bmatrix} F_1 & F_{s1y} & F_2 & F_{s2y} \end{bmatrix}^T;$$
$$T_d = \begin{bmatrix} T_{d1} & T_{d2} & T_{d3} & T_{d4} \end{bmatrix}^T;$$
$$d = \begin{bmatrix} b_1\dot{q}_1 & b_2\dot{q}_2 & b_3\dot{q}_3 & b_4\dot{q}_4 \end{bmatrix}^T;$$
$$G(q) = \begin{bmatrix} 0 & 0 & 0 & 0 \end{bmatrix}^T$$

The elements of mass matrix are:

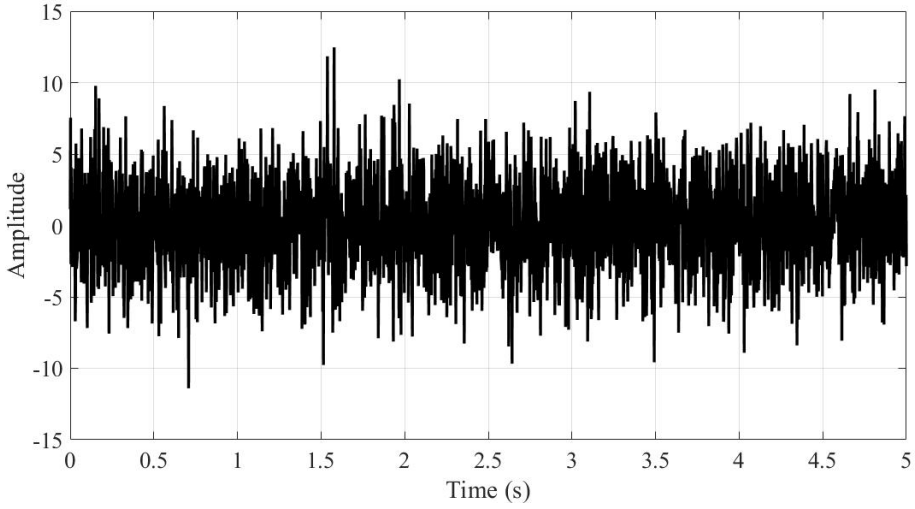

Fig. 3. External disturbance.

$$m_{11} = A_1 + A_2 + 2A_3 \cos q_2;$$
$$m_{12} = m_{21} = A_2 + A_3 \cos q_2;$$
$$m_{22} = A_2;\ m_{13} = m_{14} = m_{23} = m_{24} = 0;$$
$$m_{33} = A_4 + A_5 + 2A_6 \cos q_4;$$
$$m_{34} = m_{43} = A_5 + A_6 \cos q_4;$$
$$m_{44} = A_5;\ m_{31} = m_{32} = m_{41} = m_{42} = 0;$$

The components of damping matrix are given by:

$$c_{11} = -A_3 \sin q_2(\dot{q}_2^2 + \dot{q}_1\dot{q}_2) + b_1\dot{q}_1;$$
$$c_{21} = A_3\dot{q}_1^2 \sin q_2 + b_2\dot{q}_2;$$
$$c_{31} = -A_6 \sin q_4(\dot{q}_4^2 + \dot{q}_3\dot{q}_4) + b_3\dot{q}_3;$$
$$c_{41} = A_6\dot{q}_3^2 \sin q_4 + b_2\dot{q}_4;$$

The elements of the tranpose of Jacobian matrix are given by:

$$J_{11} = -L_1 \sin q_1 - L_2 \sin(q_1 + q_2);$$
$$J_{12} = -L_1 \cos q_1 - L_2 \cos(q_1 + q_2);$$
$$J_{21} = -L_2 \sin(q_1 + q_2);\ J_{13} = J_{14} = 0;$$
$$J_{22} = -L_2 \cos(q_1 + q_2);\ J_{23} = J_{24} = 0;$$
$$J_{33} = L_3 \sin q_3 + L_4 \sin(q_3 + q_4);$$
$$J_{34} = -L_3 \cos q_3 - L_4 \cos(q_3 + q_4);$$
$$J_{43} = L_4 \sin(q_3 + q_4);\ J_{31} = J_{32} = 0;$$
$$J_{44} = -L_4 \cos(q_3 + q_4);\ J_{41} = J_{42} = 0;$$

The term used in the equations of motion of the robot arms:

$$A_1 = m_1k_1^2 + m_2l_1^2 + I_1;$$
$$A_2 = m_2k_2^2 + I_2;\ A_3 = m_2l_1k_2;$$
$$A_4 = m_3k_3^2 + m_4l_3^2 + I_3;$$
$$A_5 = m_4{k_4}^2 + I_4;\ A_6 = m_4l_3k_4$$

References

[1] C. Park, K. Park, and D. Kim, "Design of dual arm robot manipulator for precision assembly of mechanical parts," in *2008 International Conference on Smart Manufacturing Application*. IEEE, 2008, pp. 424–427.

[2] H. M. Do, C. Park, T. Y. Choi, and J. H. Kyung, "Design and control of dual-arm robot for cell manufacturing process," in *2013 IEEE International Conference on Mechatronics and Automation*. IEEE, 2013, pp. 1419–1423.

[3] P. Tsarouchi, S. Makris, G. Michalos, M. Stefos, K. Fourtakas, K. Kaltsoukalas, D. Kontrovrakis, and G. Chryssolouris, "Robotized assembly process using dual arm robot," *Procedia CIrP*, vol. 23, pp. 47–52, 2014.

[4] M. J. Bakari, K. M. Zied, and D. W. Seward, "Development of a multi-arm mobile robot for nuclear decommissioning tasks," *International Journal of Advanced Robotic Systems*, vol. 4, no. 4, p. 51, 2007.

[5] M. Gharbi, J. Cortés, and T. Siméon, "Roadmap composition for multi-arm systems path planning," in *2009 IEEE/RSJ International Conference on Intelligent Robots and Systems*. IEEE, 2009, pp. 2471–2476.

[6] M. Fridin and M. Belokopytov, "Acceptance of socially assistive humanoid robot by preschool and elementary school teachers," *Computers in Human Behavior*, vol. 33, pp. 23–31, 2014.

[7] J. T. Wen and K. Kreutz-Delgado, "Motion and force control of multiple robotic manipulators," *Automatica*, vol. 28, no. 4, pp. 729–743, 1992.

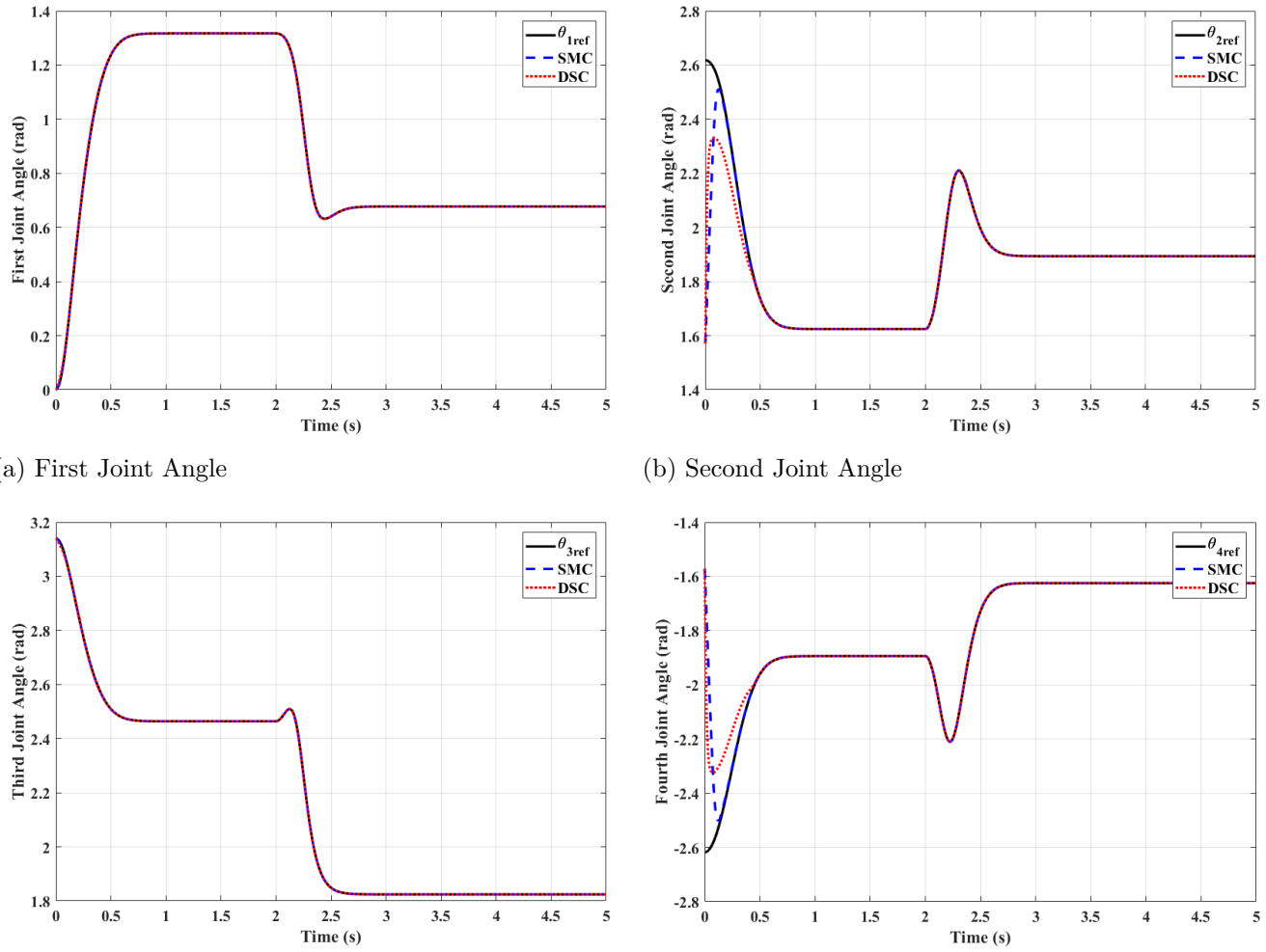

(a) First Joint Angle

(b) Second Joint Angle

(c) Third Joint Angle

(d) Fourth Joint Angle

Fig. 4. Motion of DAR links.

[8] V. Perdereau and M. Drouin, "Hybrid external control for two robot coordinated motion," *Robotica*, vol. 14, no. 2, pp. 141–153, 1996.

[9] F. Caccavale, P. Chiacchio, A. Marino, and L. Villani, "Six-dof impedance control of dual-arm cooperative manipulators," *IEEE/ASME Transactions On Mechatronics*, vol. 13, no. 5, pp. 576–586, 2008.

[10] J. Lee, P. H. Chang, and R. S. Jamisola, "Relative impedance control for dual-arm robots performing asymmetric bimanual tasks," *IEEE transactions on industrial electronics*, vol. 61, no. 7, pp. 3786–3796, 2014.

[11] V. Utkin, J. Guldner, and J. Shi, *Sliding mode control in electro-mechanical systems*. CRC press, 2009.

[12] N. Yagiz, Y. Hacioglu, and Y. Z. Arslan, "Load transportation by dual arm robot using sliding mode control," *Journal of Mechanical science and Technology*, vol. 24, no. 5, pp. 1177–1184, 2010.

[13] Y. Hacioglu, Y. Z. Arslan, and N. Yagiz, "Mimo fuzzy sliding mode controlled dual arm robot in load transportation," *Journal of the Franklin Institute*, vol. 348, no. 8, pp. 1886–1902, 2011.

[14] Y. H. Joo, L. Q. Tien, P. X. Duong *et al.*, "Adaptive neural network second-order sliding mode control of dual arm robots," *International Journal of Control, Automation and Systems*, vol. 15, no. 6, pp. 2883–2891, 2017.

[15] Q. Hu, L. Xu, and A. Zhang, "Adaptive backstepping trajectory tracking control of robot manipulator," *Journal of the Franklin Institute*, vol. 349, no. 3, pp. 1087–1105, 2012.

[16] N. Nikdel, M. Badamchizadeh, V. Azimirad, and M. A. Nazari, "Fractional-order adaptive backstepping control of robotic manipulators in the presence of model uncertainties and external disturbances," *IEEE Transactions on Industrial Electronics*, vol. 63, no. 10, pp. 6249–6256, 2016.

[17] Y. Jiang, Z. Liu, C. Chen, and Y. Zhang, "Adaptive robust fuzzy control for dual arm

robot with unknown input deadzone nonlinearity," *Nonlinear Dynamics*, vol. 81, no. 3, pp. 1301–1314, 2015.

[18] K. Bai, M. Luo, M. Liu, and G. Jiang, "Fuzzy backstepping control for dual-arm cooperative robot grasp," in *2015 IEEE International Conference on Robotics and Biomimetics (ROBIO)*. IEEE, 2015, pp. 2563–2568.

[19] H. Zhao-bin CHEN Li, "Fuzzy neural network self-learning control of free-floating dual-arm space robot system [j]," *Robot*, no. 5, p. 10, 2008.

[20] Z. Liu, C. Chen, Y. Zhang, and C. P. Chen, "Adaptive neural control for dual-arm coordination of humanoid robot with unknown nonlinearities in output mechanism," *IEEE transactions on cybernetics*, vol. 45, no. 3, pp. 507–518, 2015.

[21] C. Yang, Y. Jiang, Z. Li, W. He, and C.-Y. Su, "Neural control of bimanual robots with guaranteed global stability and motion precision," *IEEE Transactions on Industrial Informatics*, vol. 13, no. 3, pp. 1162–1171, 2017.

[22] D. Swaroop, J. K. Hedrick, P. P. Yip, and J. C. Gerdes, "Dynamic surface control for a class of nonlinear systems," *IEEE transactions on automatic control*, vol. 45, no. 10, pp. 1893–1899, 2000.

[23] D. Wang and J. Huang, "Neural network-based adaptive dynamic surface control for a class of uncertain nonlinear systems in strict-feedback form," *IEEE Transactions on Neural Networks*, vol. 16, no. 1, pp. 195–202, 2005.

[24] M.-Z. Hou and G.-R. Duan, "Robust adaptive dynamic surface control of uncertain nonlinear systems," *International Journal of Control, Automation and Systems*, vol. 9, no. 1, pp. 161–168, 2011.

Anh Tuan Phan, photograph and biography not available at the time of publication.

Huu Nguyen Thai, photograph and biography not available at the time of publication.

Cong Khoa Nguyen, photograph and biography not available at the time of publication.

Quang Uoc Ngo, photograph and biography not available at the time of publication.

Hoai Anh Duong, photograph and biography not available at the time of publication.

Quoc Truong Vo, photograph and biography not available at the time of publication.

DOI:10.4186/ej.2020.24.3.159

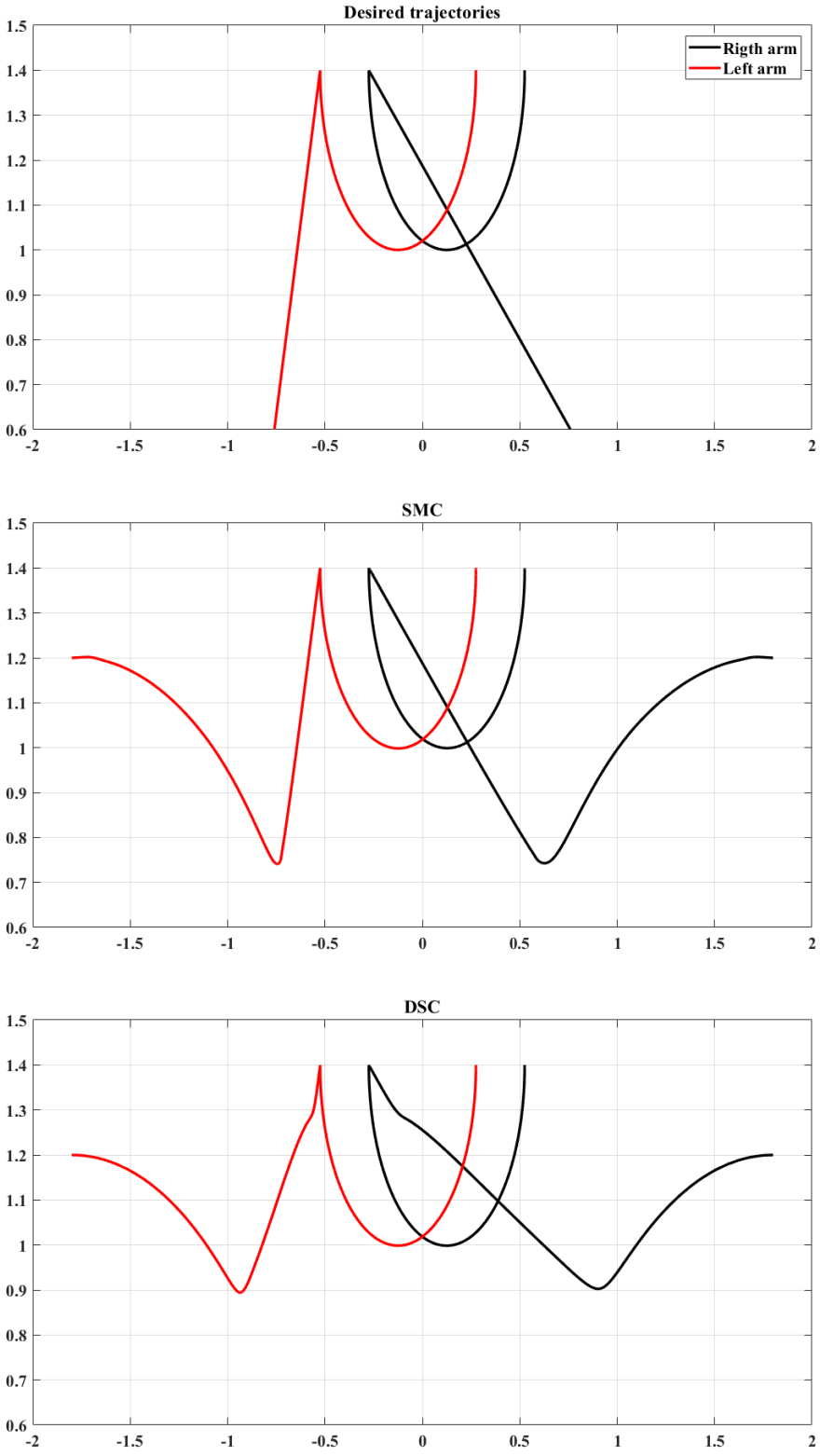

Fig. 5. Trajectories of end-effectors.